THE JOURNAL OF PHYSICAL CHEMISTRY C

Article

pubs.acs.org/JPCC

Modulating the Catalytic Activity of Cerium Oxide Nanoparticles with the Anion of the Precursor Salt

Swetha Barkam,[†] Julian Ortiz,[†] Shashank Saraf,[†] Nicholas Eliason,[†] Rameech Mccormack,[†] Soumen Das,[†,‡] Ankur Gupta,[†] Craig Neal,[†] Alex Petrovici,[§] Cameron Hanson,[§] Michael D. Sevilla,[§] Amitava Adhikary,*[,§] and Sudipta Seal*[,†,‡,∥]

[†]Advanced Materials Processing and Analysis Center (AMPAC), Materials Science and Engineering (MSE), University of Central Florida, 4000 Central Florida Boulevard, Orlando, Florida 32816, United States

[‡]NanoScience Technology Center (NSTC), Materials Science Engineering (MSE), University of Central Florida, 4000 Central Florida Boulevard, Orlando, Florida 32816, United States

[§]Department of Chemistry, Oakland University, 146 Library Drive, Rochester, Michigan 48309, United States

[∥]College of Medicine, University of Central Florida, 6850 Lake Nona Boulevard, Orlando, Florida 32827, United States

Supporting Information

ABSTRACT: In this work, we tested our hypothesis that surface chemistry and antioxidant properties of cerium nanoparticles (CNPs) are affected by the presence of counterions. We first employed various precursor cerium(III) (Ce(III)) salts with different counterions (acetate, nitrate, chloride, and sulfate) to synthesize CNPs following the same wet chemical methodology. Electron spin resonance (ESR) studies provided evidence for the formation of radicals from counterions (e.g., $NO_3^{\bullet 2-}$ from reduction of NO_3^- in CNPs synthesized from Ce(III) nitrate). Physicochemical properties of these CNPs, e.g., dispersion stability, hydrodynamic size, signature surface chemistry, superoxide dismutase (SOD)-mimetic activity, and oxidation potentials, were found to be significantly affected by the anions of the precursor salts. CNPs synthesized from Ce(III) nitrate and Ce(III) chloride exhibited higher extent of SOD-mimetic activities. Therefore, these CNPs were studied extensively employing in situ ultraviolet (UV)−visible spectroelectrochemistry and changing the counterion concentrations affecting the oxidation potentials of these CNPs. Thus, the physicochemical and antioxidant properties of CNPs can be modulated by anions of the precursor. Furthermore, our ESR studies present evidence of the formation of guanine cation radical ($G^{\bullet +}$) in 5′-dGMP via UV-photoionization at 77 K in the presence of CNPs synthesized from Ce(III) nitrate and chloride, and CNPs act as the scavenger of radiation-produced electrons.

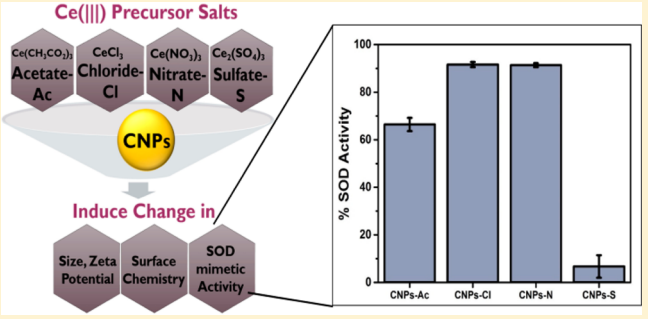

INTRODUCTION

Owing to the advanced characteristic features and properties that are attributed to their miniature size and morphology, nanoparticles have altered the face of nanotechnology. The properties of nanoparticles have generated a plethora of applications in the field of biomedicine, optics, energy science, etc.[1] Ceria nanoparticles (CNPs) have been proven to be a novel material in the field of nanomedicine; CNPs are shown to have potential applications in drug delivery systems with therapeutic abilities.[2] Revelation of the antioxidant-mimetic properties of CNPs has identified these nanoparticles as a possible therapeutic agent for pathologies related to oxidative stress.[2] Previously, ceria was known for its application in catalysis, solid oxide fuel cells, polishing, ultraviolet shielding, etc.[3−6] The nanosize property of CNPs enabled them to mimic naturally existing enzymes, such as superoxide dismutase (SOD), by scavenging and thereby modulating the levels of reactive oxygen species (ROS) in the microenvironment around the nanoparticles.[7]

Our work, as well as work in other laboratories, showed that both oxidation states of cerium (Ce^{4+} and Ce^{3+}) could coexist on the surface of CNPs.[8] The simultaneous coexistence of both oxidation states of cerium in different ratios creates oxygen vacancies, which play a crucial role in controlling the surface chemistry of CNPs.[8] Our ongoing work on CNPs established that the regenerative property of CNPs is the outcome of switching of oxidation states from Ce^{3+} to Ce^{4+} and vice versa.[8] These oxygen vacancies act as potential hotspots for pronounced catalytic activity, possessing antioxidant properties with applications in biomedicine and the healthcare industry.[9] As a result, CNPs are found to be effective against pathologies

Received: June 12, 2017
Revised: August 17, 2017
Published: August 21, 2017

DOI: 10.1021/acs.jpcc.7b05725
J. Phys. Chem. C 2017, 121, 20039−20050

associated with chronic oxidative stress (such as cancer, neurodegenerative diseases, etc.) and inflammation.[10] CNPs are well-tolerated in in vitro as well as in vivo biological models, which makes these nanoparticles suitable for nanobiology and regenerative medicine applications.[2] For example, free radical formation during cellular growth hinders cell differentiation, and the induction of angiogenesis of CNPs with a high $[Ce^{3+}]$:$[Ce^{4+}]$ ratio aids in wound-healing applications by promoting cell growth and tissue engineering through antioxidant activity.[11]

We have shown that the characteristic properties of nanoparticles are highly susceptible to changes in its micro-environment such as pH, ionic strength, temperature, moisture, radiation light, etc., owing to the high surface energy at lower size. Furthermore, our work has provided evidence that the synthesis method and the chemistry between precursors play an equally important role in determining the physiochemical characteristics and bioactivity of CNPs.[7,12,13]

Several methods have been employed to synthesize CNPs for different applications, such as hydrothermal, spray pyrolysis, thermal hydrolysis, electrochemical synthesis, wet chemical, gas condensation, microemulsion, solvothermal, sol−gel, and sonochemical.[14] It has been previously reported that the physical (e.g., size, surface charge, agglomeration, etc.) and chemical properties (e.g., antioxidant property) of CNPs are influenced by the synthesis methods and parameters. The chemical properties of CNPs, such as its surface chemistry regulated by the surface $[Ce^{3+}]/[Ce^{4+}]$ ratio, can significantly modulate the bioactivity and antioxidant properties of CNPs.[12,15,16] We note that the protein corona formation in the biologically relevant media is regulated by the physical properties, dispersion stability as well as by the presence of any chemical entity on CNPs, thereby deciding their cellular internalization.[7,17] Therefore, it is necessary to thoroughly characterize and analyze the role of chemical entities that are present on the surface of CNPs, after the synthesis and prior to their use in biomedical applications.[12] It was already established that the high-temperature synthesis methods of CNPs resulted in larger particle size, higher size distribution, and greater degree of agglomeration.[13,14] On the other hand, room-temperature synthesis techniques, such as microemulsion and wet chemical, provided a better control on particle size distribution of CNPs and generated CNPs with lower particle size (<10 nm).[18] Wet chemical synthesis provided an advantage of generating a homogeneous distribution of small sized (3−5 nm) CNPs with stable dispersion; these CNPs were found to be adequately suitable for biomedical applications.[18] The pH of the solution can be regulated to modulate the dispersion stability of CNPs with increased suspension in acidic pH.[2,13,19−21] Generally, the ratio of surface $[Ce^{3+}]$:$[Ce^{4+}]$ concentration has been observed to be greater in CNPs synthesized via wet chemical method at room temperature.[2,13,19−21] The $[Ce^{3+}]$:$[Ce^{4+}]$ ratio at the surface of CNPs has been shown to depend extensively on the kind of oxidizing or reducing agent used for the synthesis of CNPs from cerium salts.[2,13,19−21] The CNPs synthesized employing a base, such as ammonium hydroxide or sodium hydroxide, are shown to have a high Ce^{4+} concentration on the surface ($[Ce^{3+}]$:$[Ce^{4+}]$ = 21−30%),[2,13,19−21] ehereas the CNPs synthesized in an oxidizing atmosphere of H_2O_2 are shown to have high Ce^{3+} concentration on their surface ($[Ce^{3+}]$:$[Ce^{4+}]$ = 55−65%).[2,13,19−21] Additionally, the surface chemistry of CNPs can be modified by changing the pH of the dispersion or by doping.[12]

In all the above-mentioned results, mostly cerium(III) nitrate hexahydrate salt has been used as a precursor to synthesize CNPs along with different oxidizing/reducing agents to create different physicochemical properties in CNPs. Investigations on the synthesis of CNPs using different cerium(III) precursor salts employing the same wet chemical method by H_2O_2 as well as on the physicochemical properties of these CNPs has not been reported to date. Hence, in this work, we investigated the influence of anions [e.g., acetate ($CH_3CO_2^-$), nitrate (NO_3^-), chloride (Cl^-), and sulfate (SO_4^{2-})] of the corresponding precursor cerium(III) salts on the physical and chemical properties of CNPs. The CNPs have been synthesized from these cerium(III) salts using the same wet chemical method under oxidizing environment of H_2O_2. Apart from investigation of the physical properties, the surface chemistry and the change in antioxidant properties of these CNPs have been studied. Specially, the chemistry of the anion in relation to the surface chemistry of CNPs and its antioxidant properties have been investigated employing in situ ultraviolet (UV)−visible spectroelectrochemical analysis. In addition, CNPs synthesized from cerium(III) chloride were found to be electron spin resonance (ESR) mute; hence, the CNPs synthesized from cerium(III) chloride are proposed to be suitable for radiation chemical studies of biomolecules (e.g., DNA) employing ESR spectroscopy.

The values of the redox potentials of the four DNA bases show that the most readily oxidizable base is guanine (G). In DNA, the redox potential of G is shown to be modulated by the local sequence. Mechanistic studies have shown that guanine cation radical ($G^{\bullet+}$) is involved as an intermediate in the formation oxidative lesions produced from guanine.[21−33] For example, 8-oxo-dGuo is the well-studied oxidative lesion derived from $G^{\bullet+}$.[23−25] Furthermore, $G^{\bullet+}$ is an important intermediate in DNA radiation damage that includes the radiation-induced charge-transfer processes in DNA.[22−25,30−33] As a result, following our ongoing work on studies of various types of DNA-radicals employing ESR,[22−29] we have provided the evidence of formation of $G^{\bullet+}$ in the presence of CNPs.

MATERIALS AND METHODS

Synthesis of CNPs from Different Cerium Salts. Five different CNPs have been synthesized using five different cerium salts, viz. cerium(III) acetate hydrate ($Ce^{3+}(CH_3CO_2^-)_3{\cdot}xH_2O$) 99.99% (trace metals basis), ceric ammonium nitrate ($(NH_4)_2[(Ce(NO_3)_6)]$), cerium chloride heptahydrate ($CeCl_3{\cdot}7H_2O$) 99.999% (trace metals basis), cerium nitrate hexahydrate ($Ce(NO_3)_3{\cdot}6H_2O$) 99.999% (trace metals basis), and cerium sulfate octahydrate ($Ce_2(SO_4)_3{\cdot}8H_2O$) 99.999% (trace metals basis). These cerium salts have been procured from Sigma-Aldrich, and all of them have been used without any further purification. All CNPs have been synthesized employing the same wet chemical synthesis as described previously (Scheme 1).[34] The precursor salt solutions have been oxidized with the aid of the oxidizing agent (H_2O_2) to form the homogeneous dispersion of 5 mM CNPs. The final concentration of each CNPs has been maintained to be 5 mM via addition of the requisite amount of precursor salt. Subsequently, all CNPs samples have been allowed to stabilize in the dark for 30 days prior to the investigations of their physiochemical properties.

DOI: 10.1021/acs.jpcc.7b05725
J. Phys. Chem. C 2017, 121, 20039−20050

Scheme 1. Schematic Representation of CNPs Synthesis by Wet Chemical Method Employing H_2O_2 as the Oxidizing Agent

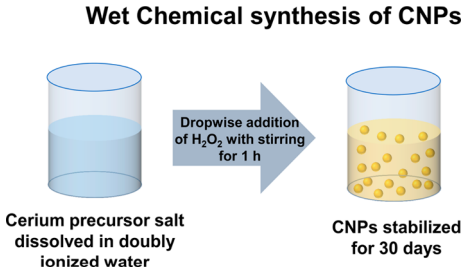

Characterization of CNPs. Following our ongoing work,[12] the hydrodynamic size and zeta potential were measured using Zeta Sizer Nano (Malvern Instruments). The Zeta sizer uses the dynamic light scattering (DLS) technique which operates using a laser of 633 nm wavelength. High-resolution transmission electron microscopy (HR-TEM) images have been obtained using Philips (Tecnai Series) TEM operating at 300 kV. Lambda 750S UV/vis spectrometer (PerkinElmer) has been used to obtain UV−visible spectra. A 10 mm path length quartz cuvette has been employed to perform the UV−visible spectral measurements. The surface chemistry illustrated by the concentration of Ce^{3+} has been calculated from the X-ray photoelectron spectroscopy (XPS) spectra of Ce 3d using a 5400 PHI ESCA (XPS) spectrometer. The Mg Kα X-ray radiation (1253.6 eV) has been used at a power of 300 W for recording the XPS measurements at a base pressure of 10^{-9} Torr. A reference peak of C 1s at 284.8 eV has been employed to compensate any peak shift due to charging effects.[12] The XPS data has been plotted as the average of three repetitions.

Analysis of SOD-Mimetic Activity. As per our ongoing work,[12] a superoxide dismutase assay kit was used to measure the SOD-mimetic activity of all the CNPs. The kit uses a water-soluble tetrazolium reagent salt, WST-1 that converts into a formazan dye upon reduction in the presence of superoxide anion radical ($O_2^{\bullet-}$). FLUOstar Omega (BMG labtech) UV−visible spectroscopy has been used to measure the absorbance of WST-1 formazan dye at 440 nm in a 96 well plate. The kinetics of this reaction has been recorded up to 30 min and analyzed for their percent antioxidant SOD-mimetic activity by employing 1 mM CNPs solutions. We have employed pure water as a control sample because it does not exhibit any SOD-mimetic activity.[12] All the SOD-mimetic activity assay analyses have been carried out based on four repetitions of the experiment (4 wells of the 96-well plate used for each sample inside a UV−visible spectroscopy plate reader). All SOD mimetic assay experiments have been conducted in aqueous medium and no buffer solutions were used for any of the experiments.

In Situ UV−Visible Spectroelectrochemical Measurements. Following the methodology in ref 35, UV−visible spectroelectrochemical measurements have been performed to gauge the change in surface chemistry in the presence of different anions via oxidizing the solutions with the aid of simultaneous application of voltage to the CNPs solutions. A Lambda 750S UV/vis spectrometer (PerkinElmer) has been employed to perform the experiments in which the sample cuvette has an electrochemical cell setup. Bio-Logic SA, Model VSP potentiostat has been used to record the electrochemical measurements. Note that the electrochemical cell setup comprises a reference, a counter, as well as a working electrode. The components of the cell were Ag/AgCl electrode as the reference electrode, thin platinum mesh of 1 cm × 0.7 cm as the working electrode, and a thin platinum wire as the counter electrode; these electrodes have been placed inside the UV−visible cuvette.[35] The cuvette used in our experiments has a path length of 2 mm. The autozero corrections have been performed to eliminate the effects of all the electrodes inside the cuvette before resuming the experiments. The open-circuit potentials have been measured inside the cuvette by recording the potentials for 20 min until the value reaches the equilibrium. Chrono-amperometry has been performed by applying a constant voltage for 3 min along with simultaneous recording of the UV−visible spectrum.

Electron Spin Resonance Spectroscopic Studies. We have carried out the electron spin resonance studies by following our well-established procedure of (a) preparation of transparent homogeneous glassy samples, (b) UV- and γ-irradiation of these samples, and (c) recording of ESR spectra of these irradiated samples followed by analyses and interpretation of the ESR spectra.[22−29]

Compounds Purchased. Lithium chloride (LiCl) (ultra dry, 99.995% (metals basis)) and lithium bromide (LiBr) (anhydrous, 99.99% (metals basis)) have been obtained from Alfa Aesar (Ward Hill, MA). 2′-Deoxyguanosine 5′-monophosphate (5′-dGMP) has been obtained from Sigma-Aldrich (St Louis, MO). Potassium persulfate (crystal) and sodium nitrate have been purchased from Mallinckrodt, Inc. (Paris, KY). All compounds were used without further purification. We chose to use CNPs generated from cerium chloride and cerium nitrate for our ESR spectral studies.

Glassy Sample Preparation. (i) Preparation of Homogeneous Solutions. To test whether CNPs exhibit ESR spectra, at first, we have prepared homogeneous solutions by mixing 250 μL of 5 mM CNP (ca. 5 nm) synthesized from cerium(III) nitrate or from cerium(III) chloride with 250 μL of 15 M LiCl in H_2O. Thus, the concentration of LiCl became 7.5 M and that of CNPs became 2.5 mM. Thereafter, homogeneous solutions of 5′-dGMP have been prepared by dissolving 2 mg/mL of this compound in these 7.5 M LiCl solutions. The pH of these solutions have not been adjusted.[22−25,29] Separately, the homogeneous solutions of $NaNO_3$ have been prepared by dissolving $NaNO_3$ at a concentration of 1 mg/mL in 7 M LiBr. In addition, following our earlier works,[22−28] the separate homogeneous solutions of 5′-dGMP (2 mg/mL) in 7.5 M LiCl/H_2O have been prepared in the presence of excess $K_2S_2O_8$ (6−8 mg/mL). $K_2S_2O_8$ scavenges the radiation-produced electrons and thus enables the investigation of the formation of only the cation radicals and the subsequent reactions of these cation radicals.

(ii) Preparation of Glassy Samples and Their Storage. At first, these homogeneous solutions have been thoroughly bubbled with nitrogen gas. Subsequently, those solutions have been immediately drawn into 4 mm Suprasil quartz tubes (Catalog no. 734-PQ-8, Wilmad Glass Co., Inc., Buena, NJ). The quartz tubes containing these solutions are then rapidly immersed in liquid nitrogen (77 K). Owing to rapid cooling at 77 K, the homogeneous liquid solutions turned into transparent homogeneous glassy solutions. All the glassy samples were stored in the dark at 77 K in Teflon containers.

UV-Irradiation of Glassy Samples and Their Storage. A helical quartz low-pressure argon−mercury vapor lamp (90% emission at 254 nm) has been employed for UV-irradiation of

DOI: 10.1021/acs.jpcc.7b05725
J. Phys. Chem. C 2017, 121, 20039−20050

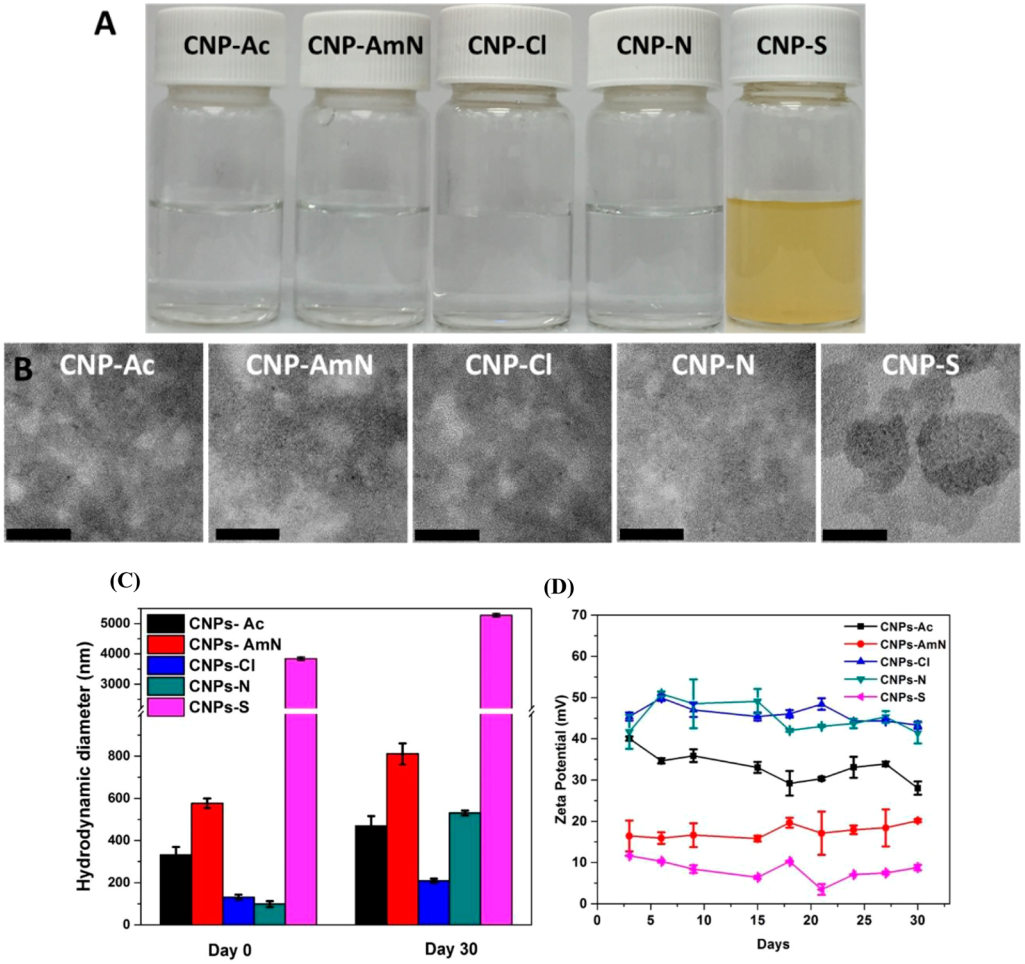

Figure 1. (A) Solutions of CNPs synthesized using cerium acetate (CNPs-Ac), cerium ammonium nitrate (CNPs-AmN), cerium chloride (CNPs-Cl), cerium nitrate (CNPs-N), and cerium sulfate (CNPs-S) as precursors. All of the CNPs solutions appear to be stable as they do not exhibit any turbidity or precipitation except for CNPs-S which shows turbidity and precipitation, indicating dispersion instability. (B) Transmission electron microscopy (TEM) images of CNPs-Ac, CNPs-AmN, CNPs-Cl, CNPs-N, and CNP-S. The bar represents a scale of 20 nm in all the TEM images. The images represent the crystallinity of CNPs synthesized from all different precursors. (C) Size and (D) zeta potential of the nanoparticles have been investigated over a period of 30 days to observe the dispersion stability of the nanoparticles using DLS.

glassy samples having CNPs and 5′-dGMP for a few minutes (2−5 min) at 77 K. These UV-irradiated glassy samples have been stored at 77 K in Teflon containers in the dark.

γ-Irradiation of Glassy Samples and Their Storage. Following our ongoing work on radicals formed in irradiated DNA and RNA-models,[22−29,31] the glassy samples of KNO_3 in 7 M LiBr/D_2O and those of 5′-dGMP in 7.5 M LiCl/H_2O in the presence of $K_2S_2O_8$ have been $\gamma(^{60}Co)$-irradiated at 77 K with absorbed doses of 500 Gy and 2.5 kGy. After γ-irradiation, these samples have been stored at 77 K in Teflon containers in the dark.

Annealing of Glassy Samples. As per our ongoing work on formation of DNA-base cation radicals,[22−28,31,36−38] the γ-irradiated (77 K) glassy (7.5 M LiCl/H_2O) sample of 5′-dGMP with $K_2S_2O_8$ has been annealed at ca. 150 K for 15 min employing a variable temperature assembly that passes liquid nitrogen-cooled dry nitrogen gas past a thermister and over it.

Electron Spin Resonance. Following our previous works,[22−29,31,36−38] a Varian Century Series X-band (9.3 GHz) ESR spectrometer with an E-4531 dual cavity, 9 in. magnet, and a 200 mW Klystron was used for the ESR studies. For the field calibration, Fremy's salt (g_{center} = 2.0056, A(N) = 13.09 G) was employed. All ESR spectra were recorded at 77 K and at microwave power of 40 dB (20 μW). Recording of ESR spectra at 77 K maximizes the signal height and allows for comparison of signal intensities. For recording and digital storage of EPR spectra and for spectral analyses, we used our in-house developed programs (ESRTAK and ESRADSUB). To obtain a simulated spectrum that matches the corresponding experimentally recorded spectrum, we employed the Bruker programs WIN-EPR and SIMFONIA.[22−29,31,36−38]

RESULTS AND DISCUSSION

Synthesis and Characterization of CNPs Synthesized Using Different Precursor. In this work, at first, we have synthesized CNPs from different cerium(III) precursor salts with different counterions (e.g., acetate ($CH_3CO_2^-$), nitrate (NO_3^-), chloride (Cl^-), and sulfate (SO_4^{2-})) using the same wet chemical method (see Materials and Methods). Subsequently, the time-based physiochemical characterizations of the CNPs have been performed to observe the changes in size and zeta potential during the stabilization period of 30 days. The data provided a deep insight into the dispersion stability of these CNPs. These results allowed us to elucidate the mechanism via which these CNPs exhibit their antioxidant properties.

DOI: 10.1021/acs.jpcc.7b05725
J. Phys. Chem. C 2017, 121, 20039−20050

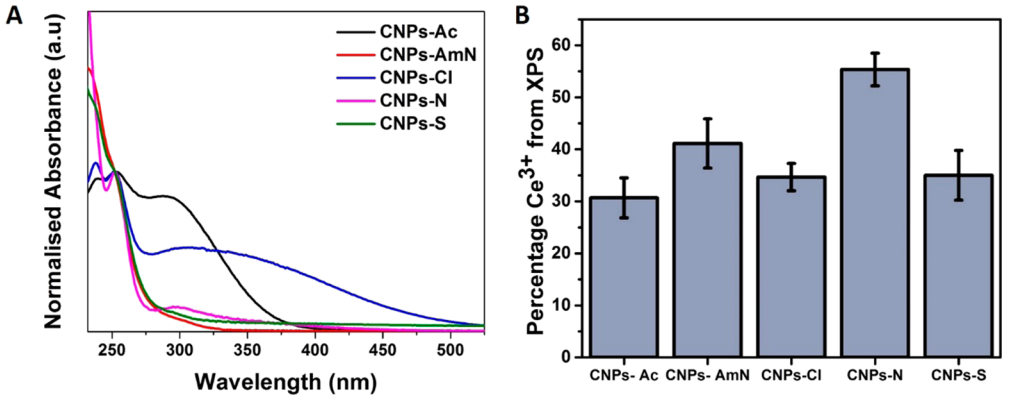

Figure 2. (A) UV−visible spectra of different CNPs after 30 days of their synthesis. This indicates that the ratio of $[Ce^{3+}]/[Ce^{4+}]$ are more dominant in case of CNPs-Ac, CNPs-Cl and CNPs-N. In the case of both CNPs-AmN and CNPs-S, the Ce^{3+} peak intensity is more prominent compared to Ce^{4+} peak, which is almost insignificant in intensity. (B) The XPS results indicate that the $\%Ce^{3+}$ on the surface of CNPs is higher in the case of CNPs-N followed by CNPs-AmN. CNPs-Cl and CNPs-S have approximately the same amount of Ce^{3+} concentration on the surface of CNPs. Furthermore, CNPs-Ac has the least amount of Ce^{3+} on the surface of the CNPs.

Figure 1 demonstrates the solutions of CNPs synthesized using cerium(III) acetate (CNPs-Ac), cerium(IV) ammonium nitrate (CNPs-AmN), cerium(III) chloride (CNPs-Cl), cerium-(III) nitrate (CNPs-N), and cerium(III) sulfate (CNPs-S). In cerium(IV) ammonium nitrate, (i) contrary to cerium(III) salts (e.g., nitrate, chloride, acetate, sulfate) used in this work as precursors, the oxidation state of cerium in this particular salt is (IV), and (ii) cerium belongs to the counterion (i.e., anion) in the complex. Therefore, it is of interest to examine how these differences affect the surface chemistry and physical properties of CNPs-AmN compared to those in CNPs-Ac, CNPs-Cl, CNPs-N, and CNP-S.

Except for solutions of CNPs-S, all other CNPs solutions appear to be stable as these solutions do not exhibit any turbidity or precipitation. CNPs-S exhibits turbidity and precipitation indicating the dispersion instability. Furthermore, initially on day 0, i.e., when the CNPs solutions were just prepared, CNPs-Cl and CNPs-N solutions were found to be transparent yellow in color; however, these CNPs solutions gradually became transparent over the duration of 30 days. We note that formation of transparent yellow color was also observed previously during synthesis of CNPs-N; on this basis, we conclude that this initial yellow color arises from the addition of H_2O_2 to cerium salts for synthesis of CNPs-Cl and CNPs-N.

Employing dynamic light scattering (DLS), we have investigated the size and the zeta potential of these CNPs over a period of 30 days in order to observe the dispersion stability of these nanoparticles. Figure 1C,D shows the change in size and zeta potential of CNPs-Ac, CNPs-AmN, CNPs-Cl, CNPs-N, and CNPs-S. It can be clearly observed that the hydrodynamic diameter of nanoparticles on day 0 was smaller compared to their increased diameter with time on day 30. All of the nanoparticles have smaller size due to dispersion stability, except CNPs-S which exhibits turbidity. Moreover, because of this turbidity in CNPs-S, the DLS measurements might not give accurate results because of scattering phenomenon, and the exposed volume of sample to the beam might not contain enough CNPs-S, as they are precipitated because of unstable dispersion stability.[39]

The zeta potentials of the nanoparticles also establish a close relation to the hydrodynamic size data; our data show that the CNPs-S has the least zeta potential which is almost constant with time. It has been established that zeta potentials of colloidal solutions of more than 30 mV are considered to be the stable dispersion of nanoparticles.[40] Our results clearly show that CNPs-S exhibits lower zeta potential with highest hydrodynamic size, thereby indicating its lowest dispersion stability. This is followed by the data from CNPs-AmN. Our data indicate that the dispersion stability of various CNPs increases in the order CNPs-S < CNPs-AmN < CNPs-Ac < CNPs-Cl ≈ CNPs-N. Therefore, we conclude that the presence of the hexanitratocerate anion ($[(Ce(NO_3)_6)]^{2-}$) in CNPs-AmN and the sulfate anion (SO_4^{2-}) in CNPs-S do significantly affect the dispersion stability of CNPs compared to dispersion stability in CNPs with the nitrate, chloride, and acetate ions.

It is well-established that the lower hydrodynamic size and higher zeta potential are indication of stable suspension of CNPs.[40] Such CNPs can possibly exhibit higher catalytic activity due to higher surface area and increased stability. On this basis, it can be inferred that CNPs-Cl, CNPs-N, and CNPs-Ac might depict higher catalytic activity, thereby indicating enhanced potential antioxidant activities. Additionally, we note here that the zeta potential values of all the CNPs do not change drastically over the duration of formation for 30 days.

Surface Chemistry of CNPs. The UV−visible spectrophotometry of cerium in CNPs provides qualitative as well quantitative information about the change in cerium oxidation states, and these results are presented in Figure 2A. The UV−visible spectra of different CNPs have been recorded after 30 days. The peaks at ca. 252 nm and at ca. 290 nm correspond to that of Ce^{3+} and Ce^{4+}, respectively, in CNPs. In the case of CNPs-Ac, the peak intensities of both Ce^{3+} and Ce^{4+} are more prominent. On the other hand, in the case of CNPs-Cl, CNPs-N, CNP-AmN, and CNPs-S, the peak of Ce^{3+} alone is more pronounced. It has been previously reported that CNPs with higher concentrations of Ce^{3+} than those with Ce^{4+} on their surface are more SOD-mimetic in nature,[9] whereas CNPs with higher concentration of Ce^{4+} than those of Ce^{3+} on their surface are more catalase-mimetic in nature.[41] On this basis, as the ratio of concentration of Ce^{3+} with that of Ce^{4+} on the surface in CNPs ($[Ce^{3+}]/[Ce^{4+}]$) are much higher in case of CNPs-Ac, CNPs-Cl, and CNPs-N, we can expect the better SOD-mimetic (antioxidant) activities from these CNPs. For CNPs-AmN and CNPs-S, the Ce^{3+} peak intensities are found to be more prominent compared to those of Ce^{4+} peaks, which

DOI: 10.1021/acs.jpcc.7b05725
J. Phys. Chem. C 2017, 121, 20039−20050

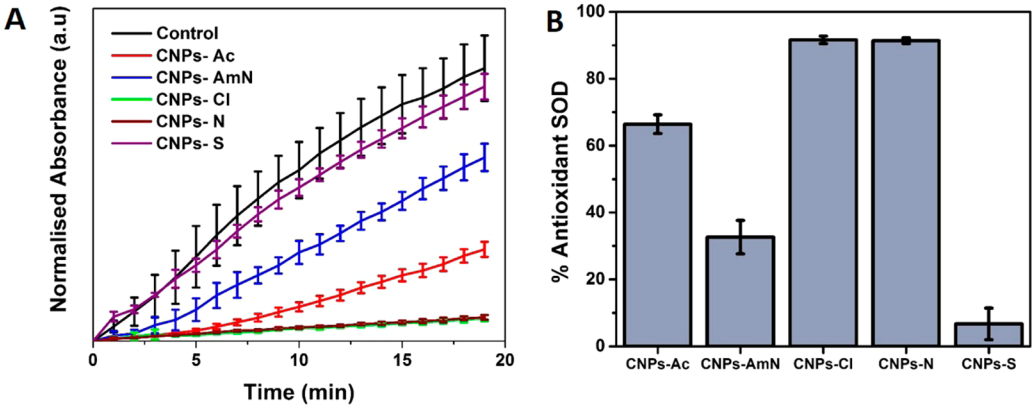

Figure 3. (A) SOD-mimetic activities of CNPs synthesized using different precursors, showing that CNPs-N and CNPs-Cl have the highest SOD-mimetic activity followed by those of CNPs-Ac. The CNPs-S and CNPs-AmN do not show high SOD-mimetic activity. Absorbance of WST-1 formazan dye at 440 nm in a 96-well plate is plotted against the time course of the reaction. (B) The percent of antioxidant capacities of CNPs do correlate with the SOD-mimetic activities of CNPs, thereby indicating the highest SOD-mimetic activities shown by CNPs-N and CNPs-Cl in panel A.

are almost insignificant in their intensities. Also, for CNPs-N and CNPs-Cl, the Ce^{3+} peak shapes have been found to be more prominent compared to the corresponding Ce^{3+} peak shapes in CNPs-AmN and CNPs-S.

The XPS analyses of CNPs synthesized using different precursors have been performed on day 30 to analyze their dynamic surface chemistry (see Figure 2B). The XPS spectrum of Ce(3d) of CNPs have been analyzed to calculate the % Ce^{3+} on the surface of the nanoparticle, as shown in Figure 2B. The results in Figure 2B show that the % Ce^{3+} on the surface of CNPs is higher in the case of CNPs-N (~55.3%) followed by that in CNPs-AmN (~41.1%). CNPs-Cl (~34.6%) and CNPs-S (~35%) have approximately the same amount of Ce^{3+} concentration on the surface of CNPs. Furthermore, CNPs-Ac (~30.6%) has the least amount of Ce^{3+} on the surface of CNPs. These results indicate that the CNPs-N should exhibit the highest SOD-mimetic activity followed by the SOD-mimetic activities of CNPs-AmN, CNPs-Cl, CNPs-S, and CNPs-Ac. However, the dispersion instability observed in CNPs-AmN and CNPs-S can affect their SOD-mimetic activities owing to the scattering effects observed during the assay of SOD-mimetic activities employing UV−visible spectroscopy.

The UV−visible spectra of all the CNPs have been plotted by normalizing the data using the Ce^{3+} peak at 252 nm. Moreover, the UV−visible spectroscopy measurements of the CNPs have been carried out in aqueous solution; on the other hand, we collected the XPS data by employing the dried form of CNPs, made by drying the nanoparticles on a silicon wafer. As a result, the UV−visible spectral results and their analysis shall intrinsically be different from those obtained the XPS analysis owing to the presence of surrounding ions and water molecules around the nanoparticles, which are absent in the case of their XPS studies. However, CNPs-Ac and CNPs-Cl show a prominent Ce^{4+} peak around 290 nm in UV−vis spectroscopy, thereby exhibiting lower % Ce^{3+} than in the XPS analysis. Both CNPs do not have much lower % Ce^{3+} in XPS compared to CNPs-N as they both still demonstrate a visible Ce^{3+} peak as well. On the other hand, CNPs-Cl exhibits predominantly a Ce^{3+} peak, attributed to the high % Ce^{3+} in XPS. Additionally, the CNPs, CNPs-S and CNPs-AmN, which exhibit dispersion instability, do demonstrate erratic UV−vis spectra in aqueous solution. Thus, we believe that the XPS data of these two CNPs might be closer to the true characterization of their surface chemistry.

Therefore, from the results shown in Figures 1 and 2, we conclude that despite using the same wet chemical synthesis method and oxidizing agent, the counterions in various cerium precursor salts can significantly alter the surface chemistry of CNPs and thereby should exhibit altered potential catalytic activities. This conclusion is well-supported by the results presented below.

SOD-Mimetic Activity of CNPs. In this study, the SOD-mimetic activities of various CNPs have been evaluated using the kit after day 30. The values of percent of SOD-mimetic activities have been estimated for different CNPs synthesized using different precursors. The SOD-mimetic activities of different CNPs are presented in Figure 3A. We note that lower curves from the water control indicate more SOD-mimetic nature. On this basis, the results presented in Figure 3A show the higher SOD-mimetic activity of CNPs-N as well as of CNPs-Cl followed by CNPs-Ac. It is clear from Figure 3A that the CNPs-S and CNPs-AmN do not exhibit high SOD-mimetic activities, which are attributed to their lower dispersion stabilities, as discussed previously. The increased scattering phenomenon of the precipitated and unstable dispersion stability of CNPs-S and CNPs-AmN samples give rise to erratic results in SOD-mimetic activity measurements using UV−visible spectroscopy. CNPs-N has the highest Ce^{3+} concentration on its surface, and it clearly correlated to the highest SOD-mimetic activity. The SOD-mimetic activity of CNPs-Cl is found to be equivalent to that of CNPs-N; thus, we conclude that CNPs-Cl does exhibit high SOD mimetic activity. However, it is intriguing that CNPs-Cl with low surface Ce^{3+} concentration exhibits high SOD-mimetic activity. It can be inferred that the presence of Cl^- could alter the catalytic antioxidant property of CNPs-Cl even though it has less concentration of Ce^{3+} on the surface. Therefore, we have performed in situ UV−visible spectroelectrochemical analysis to understand further the role of Cl^- versus NO_3^- on the surface chemistry of CNPs-Cl and CNPs-Cl. Figure 3B represents the percent of antioxidant capacity of CNPs estimated after 30 min of the assay time. The results of percent antioxidant capacities of CNPs in Figure 3B clearly correlate to the SOD-mimetic activities represented in Figure 3A.

DOI: 10.1021/acs.jpcc.7b05725
J. Phys. Chem. C 2017, 121, 20039−20050

The different sizes of CNPs generated employing the same synthesis method but using different precursor salts demonstrate the effect of the anion of the precursor salt on the nucleation and the growth kinetics of the nanoparticles during their synthesis. The overall noticeable observation is that the smaller sized nanoparticles having high surface area exhibit higher activity due to increased interaction with the target molecules. Previously, it has been established that the size of CNPs has been known to affect the surface $[Ce^{3+}]/[Ce^{4+}]$ ratio, which in turn affects the antioxidant activity of CNPs. It has been reported that the smaller sized crystalline CNPs show a higher $[Ce^{3+}]/[Ce^{4+}]$ ratio on its surface.[2,13] In our study, all the samples except CNPs-S exhibit similar size and shape. This reveals the fact that the even if CNPs have similar sizes, their surface chemistry can be varied because of the presence of the precursor anion. CNPs-S is shown to have greater size, which can be observed in the DLS characterization revealing increased size and low zeta potential (see Figure 1). The XPS data of CNPs-S shows high Ce^{4+} which is inconsistent with the previously reported data, though this observation is not exclusive for all the CNPs prepared in this study (see Figure 1).

Quantification of Enzymatic Mimetic Activity of CNPs. The rates of reaction of CNPs (CNPs-Ac, CNPs-AmN, CNPs-Cl, CNPs-N, and CNPs-S) that are pertinent to their SOD-mimetic activities have been analyzed employing the SOD-mimetic kinetics (see Figure 4). The SOD-mimetic assays have been performed using different concentrations of hypoxanthine (which produces $O_2^{\bullet-}$ upon reaction with xanthine oxidase, the substrate that binds to the enzyme CNPs in the enzymatic reaction adopted for analyzing enzymatic kinetics): 0.1, 0.5, 1, and 1.5 mM. From Figure 4 it can be observed that the rates of scavenging of $O_2^{\bullet-}$ by CNPs increase with rise in concentration of hypoxanthine. Furthermore, the data in Figure 4 show that the rates of reactions involved in the SOD-mimetic activities of CNPs-Cl and CNPs-N are the highest followed by that of CNPs-Ac. The rate of $O_2^{\bullet-}$ scavenging of CNPs-S and CNPs-AmN are found to be the lowest; these results correlate well to the dispersion stability of these CNPs. The rates have been calculated by assuming that at a particular given time, the amount of $O_2^{\bullet-}$ scavenged by CNPs is proportional to the difference between the extent of $O_2^{\bullet-}$ scavenged by WST-1 reagent in the presence of CNPs and that in the absence of CNPs (i.e., water control). The change in the rate of $O_2^{\bullet-}$ scavenging with increase in substrate concentration provides an in-depth understanding of CNPs in terms of enzymatic kinetics. This can be correlated to the Michaelis–Menten saturation curve for an enzyme reaction that shows the relation between the substrate concentration and reaction rate. The Michaelis–Menten kinetics data are presented in Figure 4. It is clearly evident from Figure 4 that the rates of $O_2^{\bullet-}$ scavenging by CNPs-N and CNPs-Cl are found to be higher than that by CNPs-Ac, whereas the corresponding rates of $O_2^{\bullet-}$ scavenging by CNPs-S and CNPs-AmN are found to be lower. These results correlate well to those already reported in Figures 1–3 for the physiochemical studies of CNPs that include investigations of hydrodynamic size, zeta potential, UV–visible spectra results, XPS analysis, and of SOD-mimetic activity.

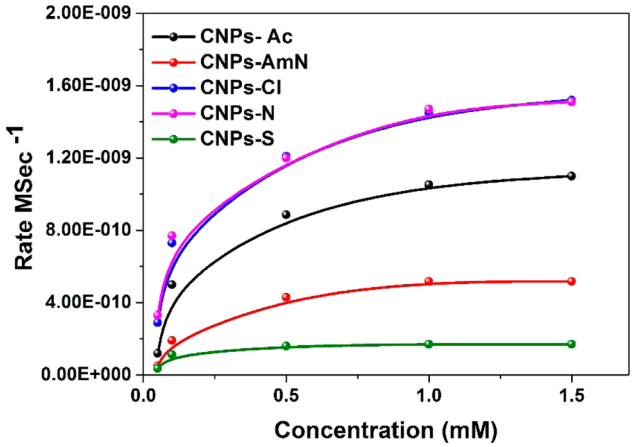

Figure 4. Michaelis–Menten kinetics of CNPs (CNPs-Ac, CNPs-AmN, CNPs-Cl, CNPs-N, and CNPs-S). The SOD-mimetic reactions were carried out by employing different concentrations of CNPs such as 0.1, 0.5, 1, and 1.5 mM.

Michaelis–Menten kinetics is one of the best-known models to quantify enzymatic kinetics in biochemistry. The model correlates the rate of the enzymatic reaction (v) with the concentration of a substrate [S], given by the formula

$$v = \frac{d[P]}{dt} = \frac{V_{max} + [S]}{K_M + [S]}$$

Here, V_{max} represents the maximum rate achieved by the enzymatic reaction, at the maximum saturating substrate concentrations. The Michaelis constant is given by K_M which is the substrate concentration at which the reaction rate is half of V_{max}. Using nonlinear regression of the Michaelis–Menten equation and the plot of the reaction rate against concentration, the values of K_M and V_{max} have been calculated. The rates of reaction ($O_2^{\bullet-}$ scavenging by CNPs) increase with the rise in the concentration of substrate, approaching V_{max} value, when all $O_2^{\bullet-}$ are scavenged by CNPs. The higher value of K_M indicates higher affinity, which means that the value of V_{max} is quickly being approached. The values of Michealis–Menten constants, K_M and V_{max}, are reported in Table 1.

The calculated enzyme-like kinetics of CNPs (see Figure 4 and Table 1) have been found to be comparable to that of SOD enzymes.[19] The second-order rate constants of SOD enzymes are calculated to be of the order of 10^9 M^{-1} sec^{-1} depending on the kind of SOD enzyme and the pH of the solution.[19] Therefore, these values are comparable to the V_{max} (reaction rates) values of CNPs-Cl, CNPs-N, and CNPs-Ac (see Table 1).

Effect of Cl^- and NO_3^- on the Enzymatic Catalytic Properties of CNPs. The effects of added Cl^- and NO_3^- on the catalytic activities of CNPs have been studied using SOD-mimetic assay and UV–visible spectro-electrochemistry analyses. These investigations would enable us to elucidate the reason behind the unusually higher SOD-mimetic activity of

Table 1. Michaelis–Menten Constants V_{max} and K_M Calculated from the Michaelis–Menten Fitted Curves Shown in Figure 4

CNPs	Ac	AmN	Cl	N	S
V_{max} (M/sec^{-1})	1.093×10^{-9}	5.11×10^{-10}	1.512×10^{-9}	1.5302×10^{-9}	1.72×10^{-10}
K_M (mM)	0.188	0.25	0.161	0.159	0.46

DOI: 10.1021/acs.jpcc.7b05725
J. Phys. Chem. C 2017, 121, 20039–20050

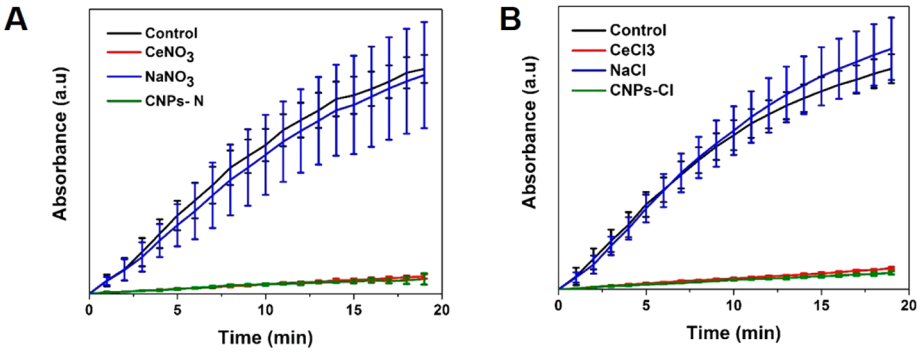

Figure 5. (A) SOD-mimetic activity of $CeNO_3$, $NaNO_3$, and CNPs-N. (B) SOD-mimetic activity of $CeCl_3$, NaCl, and CNPs-Cl. Note that the lower the curve, the higher the SOD mimetic activity.

CNPs-Cl with low concentration of Ce^{3+}. The concentration of the anions, Cl^- and NO_3^-, have been varied by adding NaCl and $NaNO_3$ at different concentrations to show the effect of the individual ions on the SOD-mimetic activities of CNPs-Cl and CNPs-N, respectively. Data of SOD assays of the ceria salts, of the CNPs-Cl with added NaCl, and of CNPs-N with added $NaNO_3$ have been analyzed. This is to confirm that the added NaCl and $NaNO_3$ by themselves are not SOD-mimetic compared to CNPs-Cl and CNPs-N. Figure 5A presents the expected results showing that $CeNO_3$ has SOD-mimetic activity due to the presence of Ce^{3+} ions in the system. $NaNO_3$ does not exhibit SOD-mimetic activity as $NO_3^-$and Na^+ ions by themselves are not SOD-active. CNPs-N is found to be SOD-mimetic as mentioned above. In Figure 5B, we can observe that $CeCl_3$ exhibits SOD-mimetic activity due to the presence of Ce^{3+} ions in the system and NaCl does not exhibit SOD-mimetic activity as Cl^- and Na^+ ions by themselves are not SOD-active. We note here that the curve corresponding to NaCl (blue color) is closer to that of control-DI water (black color), which does not exhibit any SOD mimetic activity. CNPs-Cl is found to be SOD-mimetic as mentioned previously.

Furthermore, the SOD-mimetic activities have been performed employing CNPs-N and CNPs-Cl samples by addition of different concentrations of NO_3^- (for CNPs-N) and Cl^- (for CNPs-Cl), respectively. This study can provide an in-depth understanding on the effects of the anions regarding the SOD-mimetic antioxidant properties of CNPs even though these anions themselves do not possess any SOD-mimetic activity. Figure 6 shows that the varied concentrations of 0.03, 0.3, 3, and 30 mM of NO_3^- do not have any significant effect on the SOD mimetic activity of CNPs-N samples. However, it shows that the comparable increasing addition of Cl^- has affected the SOD-mimetic activity of CNP-Cl. The effect of Cl^- is found to be comparatively more than that of NO_3^- on the SOD-mimetic activity of CNPs. These data indicate that the presence of Cl^- affects the SOD-mimetic activity of CNPs.

To understand further the impact of concentrations of Cl^- and NO_3^- on the SOD-mimetic activity of CNPs, UV−visible spectroelectrochemistry has been performed to gauge the changes in oxidation potentials of CNPs in the presence of these ions. The open-circuit potentials (OCP) values of CNPs-N have been recorded with increasing concentration of NO_3^- and those of CNPs-Cl with increasing concentrations of Cl^-. The concentrations of the added ions were varied from 0, 0.3, 3, and 30 mM. Figure 7A shows that the OCP of CNPs-N increases with rise in concentrations of NO_3^-, whereas the OCP of CNPs-Cl decreases with increase in concentrations of

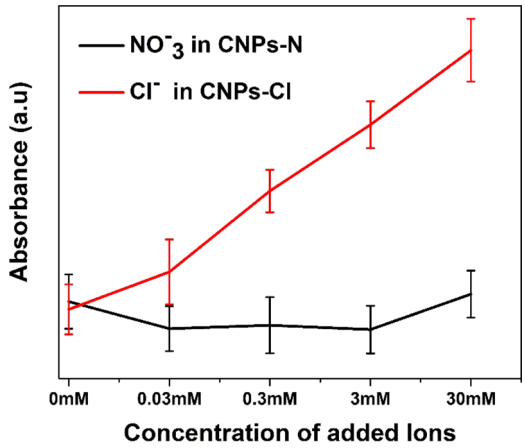

Figure 6. SOD-mimetic activity of CNPs-N with increasing concentration of NO_3^- (by the addition of $NaNO_3$ at different concentrations: 0.03, 0.3, 3, and 30 mM) and of CNPs-Cl with increasing concentration of Cl^- (by the addition of NaCl at different concentrations: 0.03, 0.3, 3, and 30 mM) at the 20th minute of SOD assay.

Cl^-. On the basis of the definition of oxidation potential, it can be inferred that in case of CNPs, if the oxidation potential is more, it is harder to oxidize those CNPs; that is, the ability to convert Ce^{3+} to Ce^{4+} in the surface of CNPs decreases. Thus, with increase in Cl^- concentrations, the oxidation potential of CNPs (Ce^{3+} converting to Ce^{4+}) decreases. This decrease points toward the increase in the ability to convert Ce^{4+} to Ce^{3+} on the surface of CNPs-Cl. On the other hand, with the increase in NO_3^- concentration, the activity and oxidation potential of CNPs-N decreases, showing the decrease in the ability to convert Ce^{4+} to Ce^{3+} on the surface of CNPs-N. This shows a drastic effect of two different ions on the oxidation potentials of these two CNPs.

Furthermore, UV−visible spectra have been recorded while applying different voltages (0, 0.1, 0.5, 0.7, 0.8 V) to the CNPs-N samples (see Supporting Information Figure S1 as well) showing an increase in the intensity of Ce^{3+} peak with rise in voltage. Addition of 30 mM NO_3^- ($NaNO_3$) to CNPs-N (see Figure S1) along with application of baseline correction, it is evident that there is not much apparent change in the peak intensities with application of voltages for CNPs-N in the case of with and without addition of excess NO_3^-. In the case of CNPs-Cl, the UV−visible spectra of Ce^{3+} peak after applying varying voltages (0, 0.1, 0.5, 0.8, 1, 1.2, and 1.5 V) are presented in Figure 7B. It can be clearly observed from Figure 7B that

DOI: 10.1021/acs.jpcc.7b05725
J. Phys. Chem. C 2017, 121, 20039−20050

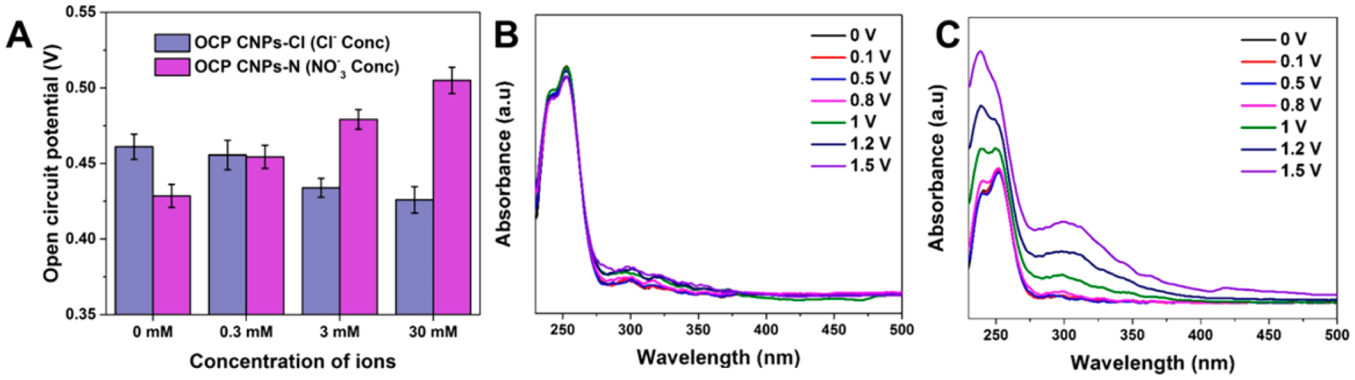

Figure 7. UV−visible spectroelectrochemical results: (A) open-circuit potentials (OCP) values of CNPs-Cl with changing concentrations of Cl^- (0, 0.3, 3, and 30 mM) and of CNPs-N with changing concentrations of NO_3^-. (B) UV−visible spectra of CNPs-Cl after applying varying voltages of 0, 0.1, 0.5, 0.8, 1, 1.2, and 1.5 V showing no change in the intensity of Ce^{3+} peak with increase in voltage. (C) UV−visible spectra of CNPs-Cl with the addition of 30 mM Cl^- after applying similar varying voltages showing an increase in the intensity. The OCP calculations were performed based on three experimental repetitions.

there is also no apparent change in the intensity of Ce^{3+} peak with increase in voltage. These results indicate that there should be no further oxidation of Ce^{3+} with the increase in voltage in CNPs-Cl. Contrary to the findings from Figure 7B, it can be inferred from the UV−visible spectra of CNPs-Cl in Figure 7C that the addition of 30 mM Cl^- ions causes an increase in the intensity with concomitant rise in voltage. This represents a clear evidence of oxidation of Ce^{3+} with the increase in voltage of the CNPs-Cl in the presence of additional Cl^- ions on the surface of CNPs-Cl. These results additionally point out that with the increase in concentration of Cl^- ions, the change in surface chemistry of CNPs-Cl is highly affected when the voltage is applied to the CNPs-Cl solutions. Thereby, it can be clearly observed that Cl^- ions indeed affect the oxidation of Ce^{3+} to Ce^{4+} in CNPs-Cl with increased intensity compared to that of NO_3^- ions in CNPs-N. This reestablishes the fact there is a clear change in the surface chemistry along with the application of voltage in the presence of two different ions in CNPs. On this basis, it can be potentially inferred that the unusual high SOD mimetic activity of CNPs-Cl, which exhibits a more Ce^{4+} concentration on its surface, is due to the altered extent of Ce^{3+} to Ce^{4+} transition in the presence of Cl^- ions.

ESR Studies. ESR studies have been carried out to test whether the anion (e.g., NO_3^-) from the precursor salt (e.g., cerium nitrate) is still present at the surface of the CNPs synthesized. CNPs-N and CNPs-Cl, which have been synthesized from two precursors, cerium(III) nitrate and cerium(III) chloride, have been chosen for ESR studies. Concentration and size of CNPs used for the ESR studies have been found to be identical (5 mM, 3−5 nm). On the basis of our findings that the DNA radicals in glassy systems (7.5 M LiBr) at low temperature undergo reactions that are similar in aqueous solutions at ambient temperatures,[21−33] we propose that CNPs should show similar surface chemistry upon rapid cooling of the aqueous solutions to liquid N_2 temperature (77 K) in glassy systems. Results of the ESR studies are shown in Figure 8.

The 2 min UV-photoionization of the 5′-dGMP sample (2 mg/mL) at 254 nm and at 77 K in 7.5 M LiCl/H_2O and in the presence of 2.5 mM CNPs that have been synthesized from the precursor salt cerium(III) nitrate has resulted in the blue spectrum shown in Figure 8A. To verify that the blue spectrum showed line components owing to $NO_3^{\bullet 2-}$, a glassy sample (7 M LiBr/D_2O) of $NaNO_3$ (1 mg/mL) was γ-irradiated

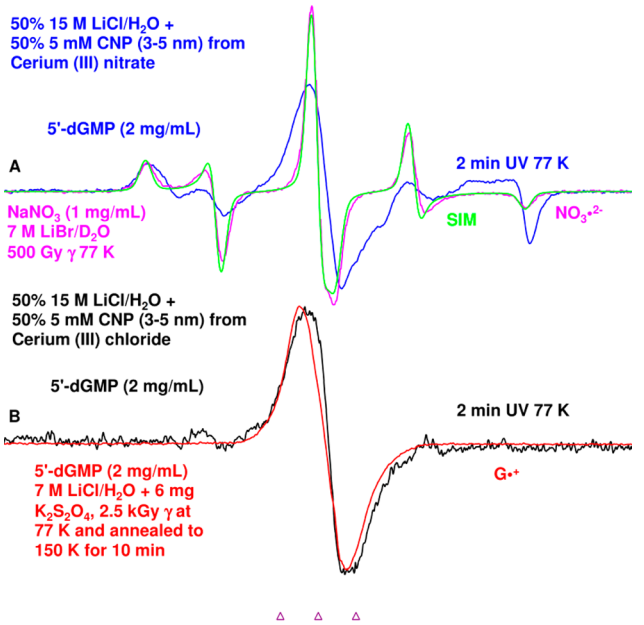

Figure 8. (A) ESR spectrum (blue) obtained after UV-photoionization at 254 nm (2 min, 77 K) of 5′-dGMP (2 mg/mL) in 7.5 M LiCl/H_2O and in the presence of 2.5 mM CNPs-N. Spectrum (pink) obtained after 77 K γ-irradiation (absorbed dose = 500 Gy) of $NaNO_3$ (1 mg/mL) in 7 M LiBr/D_2O. Green spectrum is the simulated spectrum (for simulation parameters, see text). (B) ESR spectrum (black) was obtained after UV-photoionization at 254 nm (2 min, 77 K) of 5′-dGMP (2 mg/mL) in 7.5 M LiCl/H_2O in the presence of 2.5 mM CNPs-Cl. Spectrum (red) was obtained after annealing the sample of 5′-dGMP in 7.5 M LiCl at 150 K for 10 min. This sample was originally γ-irradiated (77 K, absorbed dose = 2.5 KGy). All experimental spectra (blue, pink, black, red) were recorded at 77 K.

(absorbed dose = 500 Gy) at 77 K, and subsequently its ESR spectrum was recorded at 77 K. This spectrum (pink) is shown in Figure 8A. Instead of H_2O glass, we used the D_2O glass because it improves the spectral resolution by narrowing the line-widths. Because NO_3^- is a well-known scavenger of radiation-produced electrons forming $NO_3^{\bullet 2-}$, the green spectrum is assigned to $NO_3^{\bullet 2-}$ in a glassy system at 77 K. The radiation-produced holes led to the formation of $Br_2^{\bullet -}$, and this has been found to be ESR-mute in the spectral region (250 G).[42]

DOI: 10.1021/acs.jpcc.7b05725
J. Phys. Chem. C 2017, 121, 20039−20050

Superimposition of the pink spectrum due to $NO_3^{\bullet 2-}$ with that of the blue spectrum in Figure 8A clearly showed that the blue spectrum exhibited line components owing to $NO_3^{\bullet 2-}$. This result proved that the CNPs synthesized from cerium nitrate as precursor still contained the anion (NO_3^-) from the precursor salt. Comparison of panels A and B of Figure 8 shows that apart from the line component due to $NO_3^{\bullet 2-}$, the center of the blue spectrum in Figure 8A also has line components owing to guanine cation radical, $G^{\bullet +}$ (see eq 1 and discussion of Figure 8B, vide infra).

We note here that the pink spectrum due to $NO_3^{\bullet 2-}$ in Figure 8A has been simulated (green spectrum in Figure 8A) employing the ESR parameters A(N) = (65.8, 33.5, 33.5) G, (g_{xx}, g_{yy}, g_{zz}) = (2.001, 2.0055, 2.0055), and with a mixed (Lorentzian/Gaussian = 0.4) line width = 4 G. Superimposition of the green spectrum on the experimentally recorded pink spectrum due to $NO_3^{\bullet 2-}$ showed the nice agreement between these two spectra. We note here that isotropic N hyperfine coupling constant (HFCC) value (44.3 G) for N in $NO_3^{\bullet 2-}$ in our glassy system at 77 K is found to be in excellent agreement with those reported earlier for N in $NO_3^{\bullet 2-}$ in single crystals (A(N) = (61, 32, 32) G, (g_{xx}, g_{yy}, g_{zz}) = (2.002, 2.006, 2.006)); these earlier isotropic N HFCC value (41.7 G) corresponded to a ca. 13° deviation from planarity.[43] The nice match between the simulated spectrum (green) and the experimentally recorded spectrum (pink) of $NO_3^{\bullet 2-}$ spectrum confirms our assignments of line components due to $NO_3^{\bullet 2-}$ spectrum in the blue spectrum in Figure 8A. We note that the expected line broadening from D_2O to H_2O (compare pink spectrum with blue spectrum in Figure 8A) is indeed observed owing to larger dipolar interactions in H_2O.

The 2 min UV-photoionization of the 5′-dGMP sample (2 mg/mL) at 254 nm and at 77 K in 7.5 M LiCl/H_2O and in the presence of 2.5 mM CNPs-Cl which has been synthesized from the precursor salt cerium(III) chloride, has resulted in the black spectrum shown in Figure 8B. Comparison of the black spectrum in Figure 8B with the blue spectrum in Figure 8A evidences the presence of prominent line components of $NO_3^{\bullet 2-}$ in the blue spectrum. The red spectrum, following our works on generation of $G^{\bullet +}$ via one-electron oxidation by $Cl_2^{\bullet -}$ in the homogeneous supercooled glassy (7.5 M LiCl either in D_2O or in H_2O) solutions of DNA- and RNA-models containing guanine, is generated.[22−25,31] The one-electron oxidation of 5′-dGMP by $Cl_2^{\bullet -}$ has been carried out via thermal annealing at 150 K for 10 min in the dark. The red spectrum has been assigned to $G^{\bullet +}$. Comparison of this red spectrum due to $G^{\bullet +}$ with the black spectrum in Figure 8B as well as with the blue spectrum in Figure 8A evidences the formation of $G^{\bullet +}$ via photoionization of 5′-dGMP in the presence of CNPs in the glassy system (see eq 1). This is the first report showing formation of $G^{\bullet +}$ via photoionization of 5′-dGMP in the presence of CNPs in the glassy system. ESR studies on CNPs synthesized from cerium(III) nitrate showed the evidence of nitrate anion radical ($NO_3^{\bullet 2-}$) formation due to radiation-produced prehydrated electron capture by NO_3^- (see eq 2).

$$G \rightarrow G^{\bullet +} + e^- \quad (1)$$

$$NO_3^- + e^- \rightarrow NO_3^{\bullet 2-} \quad (2)$$

This result has established the presence of the anion (i.e., NO_3^-) in the surface of CNPs synthesized from cerium(III) nitrate. Radiation chemical studies on the reactivities of electrons have established that Cl^- is not a scavenger of radiation-generated electrons while NO_3^- is a very effective electron scavenger.[43] Thus, our ESR work establishes that Cl^- on the surface of CNPs-Cl does not contribute to the scavenging of radiation-produced electrons. Consequently, our ESR results point out that Ce^{4+} in the surface of the CNPs-Cl appears to be a better scavenger of radiation-produced electrons by reaction with Ce^{4+} generating more Ce^{3+} (see eq 3) on its surface than that for CNPs-N. This is because, in the case of CNPs-N, the radiation-produced electrons are predominantly scavenged by NO_3^-.

$$Ce^{4+} + e^- \rightarrow Ce^{3+} \quad (3)$$

CONCLUSIONS

In this work, we have tested our hypothesis that altering the anion of the precursor cerium salt affects significantly the physical properties and the surface chemistry of CNPs which have been synthesized using the same wet chemical method. In this work, the extensive physiochemical investigations of CNPs (CNPs-Ac, CNPs-AmN, CNPs-Cl, CNPs-N, and CNPs-S) have shown that CNPs-S and CNPs-AmN have lower zeta potentials and higher hydrodynamic sizes. These results have established that the hexanitratocerate ($[(Ce(NO_3)_6)]^{2-}$) and sulfate ions (SO_4^{2-}) alter the dispersion stability of CNPs in aqueous solutions. Our results have established that the dispersion stabilities of CNPs follow the descending order CNPs-S< CNPs-AmN< CNPs-Ac < CNPs-Cl ≈ CNPs-N. Additionally, the surface chemistry studied using UV−visible spectroscopy and XPS has been observed to be affected significantly by the presence of the anions from the precursor salt in CNPs. Furthermore, our results show that the percentage of Ce^{3+} on the surface of CNPs is higher in the case of CNPs-N followed by that of CNPs-AmN. The SOD-mimetic activity and the rates of removal of superoxide anion radical have been found to be highest for CNPs-N and CNPs-Cl followed by those for CNPs-Ac. The fact that CNPs-S and CNPs-AmN have not exhibited high SOD-mimetic activity can be attributed to their decreased dispersion stability. One of the most interesting findings in this particular study is the unusual higher SOD-mimetic activity of CNPs-Cl in spite of the low concentration of Ce^{3+} on its surface. In this study, the effects of Cl^- and NO_3^- ions on CNPs have been investigated further by employing the SOD-mimetic analysis and UV−visible spectro-electrochemistry of CNPs-Cl and CNPs-N with varying concentrations of the respective chloride and nitrate anions. Our work with CNPs-Cl shows that the presence of Cl^- alters the SOD mimetic activity, indirectly altering the surface chemistry. The OCP characterization has revealed that the increase in concentration of Cl^- ions decreases the oxidation potential of CNPs, whereas raising the concentration of NO_3^- ions in the CNPs-N solution increases the oxidation potential of CNPs-N. Most importantly, ESR studies clearly show the presence of surface counter ions (e.g., NO_3^- in CNPs-N) even in the presence of 7 M LiBr. This indicates a major breakthrough in recognizing the role of ions on the surface chemistry, oxidation potential, and antioxidant properties of CNPs. Thus, our work demonstrates the fact that even though the same synthesis method and oxidizers are used, just the change in the anion of the precursor salt can extensively change the physiochemical properties of nanoparticles.

DOI: 10.1021/acs.jpcc.7b05725
J. Phys. Chem. C 2017, 121, 20039−20050

■ ASSOCIATED CONTENT

Supporting Information

The Supporting Information is available free of charge on the ACS Publications website at DOI: 10.1021/acs.jpcc.7b05725.

SOD-mimetic activity of CNPs-N with various concentrations of NO_3^- (PDF)

■ AUTHOR INFORMATION

Corresponding Authors

*E-mail: adhikary@oakland.edu. Tel: 248-370-2094. Fax: 248-370-2321.

*E-mail: Sudipta.Seal@ucf.edu. Tel: 407-823-5277 or 407-882-1458. Fax: 407-882-1156 or 407-823-0208.

ORCID

Michael D. Sevilla: 0000-0001-8799-5458

Amitava Adhikary: 0000-0001-9024-9579

Notes

The authors declare no competing financial interest.

■ ACKNOWLEDGMENTS

A.A. and M.D.S. thank the National Cancer Institute of the National Institutes of Health (Grant R01CA045424). A.A. and M.D.S. are also grateful to Research Excellence Fund (REF) and Center for Biomedical Research (CBR) at Oakland University for support. A.A., M.D.S., and A.P. thank Honors College at Oakland University for support. S.S. thanks support from Space Florida and the National Aeronautics and Space Administration through the University of Central Florida's NASA Florida Space Grant Consortium. S.S. also acknowledges the grant from National Science Foundation [NSF EEC-1156747 (for RET supplement)].

■ REFERENCES

(1) Lohse, S. E.; Murphy, C. J. Applications of Colloidal Inorganic Nanoparticles: From Medicine to Energy. *J. Am. Chem. Soc.* **2012**, *134*, 15607−15620.

(2) Das, S.; Dowding, J. M.; Klump, K. E.; McGinnis, J. F.; Self, W.; Seal, S. Cerium Oxide Nanoparticles: Applications and Prospects in Nanomedicine. *Nanomedicine* **2013**, *8*, 1483−1508.

(3) Yang, J. C.; Kim, H.-J.; Kim, T. Study of Polishing Characteristics of Monodisperse Ceria Abrasive in Chemical Mechanical Planarization. *J. Electrochem. Soc.* **2010**, *157*, H235−H240.

(4) Rodriguez, J. A.; Graciani, J.; Evans, J.; Park, J. B.; Yang, F.; Stacchiola, D.; Senanayake, S. D.; Ma, S.; Pérez, M.; Liu, P.; et al. Water-Gas Shift Reaction on a Highly Active Inverse CeOx/Cu (111) Catalyst: Unique Role of Ceria Nanoparticles. *Angew. Chem.* **2009**, *121*, 8191−8194.

(5) Masui, T.; Yamamoto, M.; Sakata, T.; Mori, H.; Adachi, G.-Y. Synthesis of BN-coated CeO_2 Fine Powder as a New UV Blocking Material. *J. Mater. Chem.* **2000**, *10*, 353−357.

(6) Eguchi, K.; Setoguchi, T.; Inoue, T.; Arai, H. Electrical Properties of Ceria-based Oxides and Their Application to Solid Oxide Fuel Cells. *Solid State Ionics* **1992**, *52*, 165−172.

(7) Karakoti, A. S.; Munusamy, P.; Hostetler, K.; Kodali, V.; Kuchibhatla, S.; Orr, G.; Pounds, J. G.; Teeguarden, J. G.; Thrall, B. D.; Baer, D. R. Preparation and Characterization Challenges to Understanding Environmental and Biological Impacts of Ceria Nanoparticles. *Surf. Interface Anal.* **2012**, *44*, 882−889.

(8) Xu, J.; Harmer, J.; Li, G.; Chapman, T.; Collier, P.; Longworth, S.; Tsang, S. C. Size Dependent Oxygen Buffering Capacity of Ceria Nanocrystals. *Chem. Commun.* **2010**, *46*, 1887−1889.

(9) Heckert, E. G.; Karakoti, A. S.; Seal, S.; Self, W. T. The Role of Cerium Redox State in the SOD Mimetic Activity of Nanoceria. *Biomaterials* **2008**, *29*, 2705−2709.

(10) Karakoti, A.; Monteiro-Riviere, N.; Aggarwal, R.; Davis, J.; Narayan, R. J.; Self, W.; McGinnis, J.; Seal, S. Nanoceria as Antioxidant: Synthesis and Biomedical Applications. *JOM* **2008**, *60*, 33−37.

(11) Chigurupati, S.; Mughal, M. R.; Okun, E.; Das, S.; Kumar, A.; McCaffery, M.; Seal, S.; Mattson, M. P. Effects of Cerium Oxide Nanoparticles on the Growth of Keratinocytes, Fibroblasts and Vascular Endothelial Cells in Cutaneous Wound Healing. *Biomaterials* **2013**, *34*, 2194−2201.

(12) Barkam, S.; Das, S.; Saraf, S.; McCormack, R.; Richardson, D.; Atencio, L.; Moosavifazel, V.; Seal, S. The Change in Antioxidant Properties of Dextran-Coated Redox Active Nanoparticles Due to Synergetic Photoreduction−Oxidation. *Chem. - Eur. J.* **2015**, *21*, 12646−12656.

(13) Deshpande, S.; Patil, S.; Kuchibhatla, S. V.; Seal, S. Size Dependency Variation in Lattice Parameter and Valency States in Nanocrystalline Cerium Oxide. *Appl. Phys. Lett.* **2005**, *87*, 133113.

(14) Sun, C.; Li, H.; Chen, L. Nanostructured Ceria-based Materials: Synthesis, Properties, and Applications. *Energy Environ. Sci.* **2012**, *5*, 8475−8505.

(15) Dowding, J. M.; Das, S.; Kumar, A.; Dosani, T.; McCormack, R.; Gupta, A.; Sayle, T. X.; Sayle, D. C.; von Kalm, L.; Seal, S.; et al. Cellular Interaction and Toxicity Depend on Physicochemical Properties and Surface Modification of Redox-active Nanomaterials. *ACS Nano* **2013**, *7*, 4855−4868.

(16) Zhang, F.; Jin, Q.; Chan, S.-W. Ceria Nanoparticles: Size, Size Distribution, and Shape. *J. Appl. Phys.* **2004**, *95*, 4319−4326.

(17) Lynch, I.; Dawson, K. A. Protein-nanoparticle Interactions. *Nano Today* **2008**, *3*, 40−47.

(18) Das, S.; Singh, S.; Dowding, J. M.; Oommen, S.; Kumar, A.; Sayle, T. X.; Saraf, S.; Patra, C. R.; Vlahakis, N. E.; Sayle, D. C.; et al. The Induction of Angiogenesis by Cerium Oxide Nanoparticles Through the Modulation of Oxygen in Intracellular Environments. *Biomaterials* **2012**, *33*, 7746−7755.

(19) Korsvik, C.; Patil, S.; Seal, S.; Self, W. T. Superoxide Dismutase Mimetic Properties Exhibited by Vacancy Engineered Ceria Nanoparticles. *Chem. Commun.* **2007**, 1056−1058.

(20) Celardo, I.; De Nicola, M.; Mandoli, C.; Pedersen, J. Z.; Traversa, E.; Ghibelli, L. Ce^{3+} Ions Determine Redox-dependent Anti-apoptotic Effect of Cerium Oxide Nanoparticles. *ACS Nano* **2011**, *5*, 4537−4549.

(21) Kumar, A.; Babu, S.; Karakoti, A. S.; Schulte, A.; Seal, S. Luminescence Properties of Europium-doped Cerium Oxide Nanoparticles: Role of Vacancy and Oxidation States. *Langmuir* **2009**, *25*, 10998−11007.

(22) Adhikary, A.; Kumar, A.; Becker, D.; Sevilla, M. D. The Guanine Cation Radical: Investigation of Deprotonation States by ESR and DFT. *J. Phys. Chem. B* **2006**, *110*, 24171−24180.

(23) Adhikary, A.; Khanduri, D.; Sevilla, M. D. Direct Observation of the Hole Protonation State and Hole Localization Site in DNA-oligomers. *J. Am. Chem. Soc.* **2009**, *131*, 8614−8619.

(24) Adhikary, A.; Kumar, A.; Munafo, S. A.; Khanduri, D.; Sevilla, M. D. Prototropic Equilibria in DNA Containing One-electron Oxidized GC: Intra-duplex vs. Duplex to Solvent Deprotonation. *Phys. Chem. Chem. Phys.* **2010**, *12*, 5353−5368.

(25) Khanduri, D.; Adhikary, A.; Sevilla, M. D. Highly oxidizing excited states of one-electron-oxidized guanine in DNA: Wavelength and pH dependence. *J. Am. Chem. Soc.* **2011**, *133*, 4527−4537.

(26) Adhikary, A.; Kumar, A.; Khanduri, D.; Sevilla, M. D. Effect of Base Stacking on the Acid− Base Properties of the Adenine Cation Radical [A•+] in Solution: ESR and DFT Studies. *J. Am. Chem. Soc.* **2008**, *130*, 10282−10292.

(27) Adhikary, A.; Kumar, A.; Rayala, R.; Hindi, R. M.; Adhikary, A.; Wnuk, S. F.; Sevilla, M. D. One-electron oxidation of Gemcitabine and Analogs: Mechanism of Formation of C3′ and C2′ Sugar Radicals. *J. Am. Chem. Soc.* **2014**, *136*, 15646−15653.

(28) Adhikary, A.; Kumar, A.; Bishop, C. T.; Wiegand, T. J.; Hindi, R. M.; Adhikary, A.; Sevilla, M. D. π-Radical to σ-radical Tautomerization

in One-electron-oxidized 1-Methylcytosine and its Analogs. *J. Phys. Chem. B* **2015**, *119*, 11496−11505.
(29) Mudgal, M.; Rishi, S.; Lumpuy, D. A.; Curran, K. A.; Verley, K. L.; Sobczak, A. J.; Dang, T. P.; Sulimoff, N.; Kumar, A.; Sevilla, M. D.; et al. Prehydrated One-Electron Attachment to Azido-Modified Pentafuranoses: Aminyl Radical Formation, Rapid H-Atom Transfer and Subsequent Ring Opening. *J. Phys. Chem. B* **2017**, *121*, 4968−4980.
(30) von Sonntag, C. *Free-Radical-Induced DNA Damage and Its Repair*; Springer-Verlag: Berlin, 2006.
(31) Adhikary, A.; Becker, D.; Sevilla, M. D. Electron Spin Resonance of Radicals in Irradiated DNA. In *Applications of EPR in Radiation Research*; Lund, A., Shiotani, M., Eds.; Springer International Publishing: Heidelberg, 2014; pp 299−352.
(32) Cadet, J.; Davies, K. J. Oxidative DNA Damage & Repair: An Introduction. *Free Radical Biol. Med.* **2017**, *107*, 2−12.
(33) Dizdaroglu, M. Oxidatively Induced DNA Damage and its Repair in Cancer. *Mutat. Res., Rev. Mutat. Res.* **2015**, *763*, 212−245.
(34) Hirst, S. M.; Karakoti, A. S.; Tyler, R. D.; Sriranganathan, N.; Seal, S.; Reilly, C. M. Anti-inflammatory Properties of Cerium Oxide Nanoparticles. *Small* **2009**, *5*, 2848−2856.
(35) Otero, T. F.; Bengoechea, M. UV−visible Spectroelectrochemistry of Conducting Polymers. Energy Linked to Conformational Changes. *Langmuir* **1999**, *15*, 1323−1327.
(36) Banyasz, A.; Ketola, T.-M.; Munoz-Losa, A.; Rishi, S.; Adhikary, A.; Sevilla, M. D.; Martinez-Fernandez, L.; Improta, R.; Markovitsi, D. UV-Induced Adenine Radicals Induced in DNA A-Tracts: Spectral and Dynamical Characterization. *J. Phys. Chem. Lett.* **2016**, *7*, 3949−3953.
(37) Adhikary, A.; Kumar, A.; Palmer, B. J.; Todd, A. D.; Heizer, A. N.; Sevilla, M. D. Reactions of 5-Methylcytosine Cation Radicals in DNA and Model Systems: Thermal Deprotonation from the 5-Methyl Group vs. Excited State Deprotonation from Sugar. *Int. J. Radiat. Biol.* **2014**, *90*, 433−445.
(38) Adhikary, A.; Kumar, A.; Heizer, A. N.; Palmer, B. J.; Pottiboyina, V.; Liang, Y.; Wnuk, S. F.; Sevilla, M. D. Hydroxyl Ion Addition to One-electron Oxidized Thymine: Unimolecular Interconversion of C5 to C6 OH-adducts. *J. Am. Chem. Soc.* **2013**, *135*, 3121−3135.
(39) Langergraber, G.; Fleischmann, N.; Hofstaedter, F. A Multivariate Calibration Procedure for UV/VIS Spectrometric Quantification of Organic Matter and Nitrate in Wastewater. *Water Sci. Technol.* **2003**, *47*, 63−71.
(40) Freitas, C.; Müller, R. H. Effect of Light and Temperature on Zeta Potential and Physical Stability in Solid Lipid Nanoparticle (SLN) Dispersions. *Int. J. Pharm.* **1998**, *168*, 221−229.
(41) Pirmohamed, T.; Dowding, J. M.; Singh, S.; Wasserman, B.; Heckert, E.; Karakoti, A. S.; King, J. E.; Seal, S.; Self, W. T. Nanoceria Exhibit Redox State-dependent Catalase Mimetic Activity. *Chem. Commun.* **2010**, *46*, 2736−2738.
(42) Messer, A.; Carpenter, K.; Forzley, K.; Buchanan, J.; Yang, S.; Razskazovskii, Y.; Cai, Z.; Sevilla, M. D. Electron Spin Resonance Study of Electron Transfer Rates in DNA: Determination of the Tunneling Constant β for Single-step Excess Electron Transfer. *J. Phys. Chem. B* **2000**, *104*, 1128−1136.
(43) Atkins, P. W.; Symons, M. *The structure of inorganic radicals*; Elsevier Publishing Company: Amsterdam, 1967.

DOI: 10.1021/acs.jpcc.7b05725
J. Phys. Chem. C 2017, 121, 20039−20050